



HAL
open science

Shape optimization of braced frames for tall timber buildings: Influence of semi-rigid connections on design and optimization process

Koliann Mam, Cyril Douthe, Robert Le Roy, François Consigny

► To cite this version:

Koliann Mam, Cyril Douthe, Robert Le Roy, François Consigny. Shape optimization of braced frames for tall timber buildings: Influence of semi-rigid connections on design and optimization process. *Engineering Structures*, 2020, 216, pp.110692. 10.1016/j.engstruct.2020.110692 . hal-03490294

HAL Id: hal-03490294

<https://hal.science/hal-03490294>

Submitted on 10 May 2022

HAL is a multi-disciplinary open access archive for the deposit and dissemination of scientific research documents, whether they are published or not. The documents may come from teaching and research institutions in France or abroad, or from public or private research centers.

L'archive ouverte pluridisciplinaire **HAL**, est destinée au dépôt et à la diffusion de documents scientifiques de niveau recherche, publiés ou non, émanant des établissements d'enseignement et de recherche français ou étrangers, des laboratoires publics ou privés.

Shape optimization of braced frames for tall timber buildings: influence of semi-rigid connections on design and optimization process

Koliann Mam^{(a,c)1}, Cyril Douthe^(a), Robert Le Roy^(a,b), François Consigny^(c)

(a) Laboratoire Navier, UMR 8205, ENPC, IFSTTAR, CNRS, 6-8 Av. B. Pascal, F-77455 MLV Cedex 2, Fr

(b) Laboratoire GSA (Géométrie, Structure, Architecture), ENSA Paris Malaquais, 75272 Paris Cedex 06, France

(c) Elioth (Egis Concept), SAS, 4 rue Dolorès Ibarruri, 93188 Montreuil, France

Abstract: With the recent development of timber as a viable structural material for high-rise structures, glulam braced frames have been recently introduced in lateral load-resisting systems of timber buildings. Based on a simple shape optimization problem of a braced frame, this paper explores one of the specificities of timber structures: the influence of semi-rigid connections on their overall structural behavior and design. Dowel-type connections are first studied to obtain a simplified relation between joint stiffness and axial load-carrying capacity. Then, the established local behavior law is introduced in the shape optimization process and design of a discrete braced frame subject to lateral drift constraint under wind load. The problem is solved by a COBYLA optimization method, combined with Optimality Criteria (OC) member sizing techniques. Solutions are then evaluated and compared with classical steel/concrete design. The semi-rigid behavior of connections finally leads to a significant increase in the volume of timber but also affects the optimal shape and topology of the X-braced frame compared with classical results.

Keywords: timber, high-rise building, structural optimization, semi-rigid connection, optimality criteria

1. Introduction

1.1 Context of tall timber building

Wood has recently (re)emerged as a sustainable construction material for high-rise structures, leading to a global race towards the world's tallest timber building [1-3]. This fast development fosters today an extensive review of struc-

¹ Corresponding author. E-mail address: koliann.mam@enpc.fr

tural systems and constructive principles suited to the material's specific properties and design process. While steel and concrete have shaped the city landscape for more than a century, timber cannot stand for a pure substitute, but it has to find its own structural and architectural expression [4].

While first generation of timber buildings were mainly CLT (Cross Laminated Timber) cellular walled systems, recent design proposal use glulam braced frames as part of the lateral load resisting systems of the building, as shown in **Figure 1**: Treet (49 m, Bergen, Norway, 2015), Mjøstårnet (89 m, Brumunddal, Norway 2019), 25 King (47 m, Brisbane, Australia 2018) or Silva (56 m, Bordeaux, France, completion planned in 2022).

In 2017, ADIVBOIS, an association for the development of residential timber buildings in France, explored different perspectives on the use of timber in building construction and design, including a study on three structural systems: rigid frames, CLT shear walls and a braced frame tube [5]. This research project has highlighted the particular importance of timber connections on the behavior and design of the structural systems in timber high-rises.



Figure 1 : Existing timber buildings using braced frame systems: (Left) Treet in Bergen, Norway (<https://artec.no/prosjekter/treet/>), (Middle) Mjøstårnet, in Brumunddal, Norway (<https://www.moelven.com/mjostarnet/>) and (Right) 25 King in Brisbane, Australia (<https://www.bates-smart.com/bates-smart/projects/sectors/commercial/25-king/>)

1.2 Braced frame optimization

Numerous attempts have been made to use topology optimization techniques for the design of lateral bracing systems for steel and concrete high-rise buildings.

Depending on the type of structure, two classes of topology optimization can be distinguished [6]. For discrete structures, the optimum topology or layout design problem consists of determining the optimum number, positions, size, and mutual connectivity of the structural members. For continuum structures, it aims to find the optimal density distribution of material in a fixed domain.

In the case of continuum topology optimization for bracing layout applications, a multistory frame is generally modeled by discrete steel elements with an underlying continuum mesh. The density of each element serves as the design

variable for the topology optimization problem of the bracing layout – i.e. material distribution – generally under global stiffness or compliance constraints, but also for other objectives, including eigenfrequency, buckling, etc.

To solve this problem, many techniques have been developed. Mijar *et al.* [7] introduced a formulation based on classical Voigt and Reuss mixing rules and a *Sequential Linear Programming* (SLP) method was used to optimize the topology problem. Liang proposed an *Evolutionary Structural Optimization* (ESO) approach, with a performance index based on strain energy density [8]. To improve the exploration of the design space, Baldock [9] used a *Bi-directional* ESO (BESO) allowing material that was removed early in the evolutionary process to be replaced later if found to be structurally advantageous. Baldock also considers constraints on patterns (repeatability, symmetry, etc.), to develop more aesthetically appealing designs. Using a *Solid Isotropic Material with Penalization* (SIMP) optimization approach, Stromberg *et al.* [10] explored the impact of including the beam elements of the existing frame in the analysis. For comparison of numerical results, the optimal geometry of a braced frame is analytically derived, with an energy-based method presented in Baker [11] used for member sizing. This problem acts as a guideline for the research presented in this paper. This discrete/continuum framework was extended by Beghini *et al.* [12] with the simultaneous sizing of the discrete frame elements during the continuum topology optimization procedure.

Despite the interest and efficiency of the aforementioned techniques, the interpretation of continuum solutions into feasible (discrete) designs is not always an easy thing for practitioners. To tackle this issue, and rationalize final solutions, discrete topology optimization with ruled-based approaches have been explored. Kicinger [13] uses an *Evolution Strategy* (ES) method to generate and optimize the bracing layout of a multi-story-bay steel framework. Each cell is assigned a bracing type (K, V, \, / and X bracing) and beam/column connection types (rigid or hinged), that are coded into a global chromosome representation of the structure. Using a similar bracing unit representation, Baldock [14] explores the potential of *Genetic Programming* (GP) with designs represented as trees, operated on by design modification functions (translation, rotation, repetition, scaling).

First proposed in the '60s, truss layout optimization using the “ground structure” method, has regained popularity in recent decades thanks to the development of new manufacturing techniques and optimization schemes allowing large problems to be solved [15]. But even more importantly, new methods to obtain more practical solutions have been developed, either by rationalizing the solutions obtained via layout optimization [16], or by working on the ground structure generation [17].

1.3 Connections in timber engineering

Joints are generally a critical factor in the design of timber structures: their strength can dictate the strength of the structure, their stiffness influences global deformations and member size can be determined by characteristics of the connector [18–20].

This notion has long been recognized by carpenters and timber engineers, but the risks and potential consequences on structures were mainly neglected, or rather accepted for traditional wooden construction. The development of engineered wood and improvements of manufacturing processes in the last century, made possible the construction of complex timber structures, with larger dimensions and high-strength elements [21]. In light of this, Eurocode 5 (EC5) [22] introduced approximate design formulas (principally based on the Yield Analysis Theory proposed by Johansen [23]) to estimate resistant capacity and stiffness of common timber joints with metal fasteners (nails, screws, bolts, dowels).

While these simple approaches are adequate for many applications, it is nevertheless clear for practitioners that they can become insufficient to address challenges of modern complex timber engineering, especially those structures where the load-deformation behavior needs to be precisely evaluated. In that context, further harmonization of design principles and inclusion of state-of-the-art calculation approaches for timber connection design are of crucial interest in the development of the next generation of EC5 [24].

1.4 Paper organization

In this paper, we illustrate one of the specificities of tall timber building design. Through a simple illustrative example, we examine the impact of semi-rigid connections on the shape optimization of a glulam-braced frame.

This paper is organized into four main sections. In the next section (section 2), characteristics of an axially loaded semi-rigid timber connection are first studied. To this end, we design a timber element and its dowel-type connection in order to obtain a simplified relation between joint stiffness and axial load-carrying capacity.

Then, the established local behavior law is introduced in the shape optimization process and design of a discrete braced frame subject to a tip displacement constraint under wind load, presented in section 3. This problem is solved by a two-level optimization scheme, using at low-level both FSD (*Fully Stressed Design*) and a rigorously derived OC (*Optimality Criteria*) techniques for *size optimization* [6]; and a COBYLA (*Constrained Optimization by Linear Approximation*) method to solve the global *shape optimization* [6] problem of the defined timber frame. Results are then illustrated in section 4, with a particular emphasis on the influence of timber connection stiffness on the global structural response of the structure, compared with classical steel/concrete design.

Finally, in section 5, some conclusions are drawn on the application of the proposed methodology in view of tall timber building design and construction process.

2. Axially loaded timber connections

2.1 Design and calculation of dowel type connections

Timber joints with dowel-type fasteners are commonly used in timber engineering for many structural applications. They can be designed for a large range of loads, are easy to produce and relatively straightforward to construct. The load-bearing capacity of these connections mainly depends upon the resistance of the wood to the embedding of the dowels and the resistance of the dowel to bending.

Johansen was the first to apply the theory of plasticity to describe the mechanical behavior of dowel type connectors [23]. Assuming ideal plasticity of both steel in bending and wood in compression, he derived equations by formulating the equilibrium of forces and moments for three failure modes when either the stresses in the wood reaches the plastic failure stress level, or when a combination of plastic failure in wood and dowel is attained. With minor changes and adaptations, the actual design rules of EC5 [22] – known as the *European Yield Model* – for the calculation of load-carrying capacity of timber-to-timber and steel-to-timber connections are based on Johansen’s approach.

Design equations for the stiffness of connections that are given in the current version of EC5 are very basic and can become insufficient in complex structures where the load-deformation behavior is of particular interest [25–27]. According to EC5 [22] methodology, the stiffness of a connection depends only on the density of the wood, the dowel diameter and the total number of fasteners. Thus, it is not affected by its width and therefore remains the same regardless of the failure mode, while this influence has been observed in many experiments [25].

To fill this gap, modern research focuses on the development of numerical models that are able to predict more accurately the non-linear load-displacement relationship of the connection. One of the most promising methods, both in terms of accuracy and implementation, is the modeling of the single-dowel as an elastoplastic beam on non-linear elastic foundations [27–29].

However, in the following, given the scope of this paper, we design and calculate our dowel-type connection with an approach based on EC5 [22], as it nonetheless provides a first and simple insight of the relationship between stiffness and load-carrying capacity of dowel-type joints. This simplified model will allow assessing, in a generic way, the potential contribution of connections to the overall structural stiffness of a braced timber frame, and thus its optimization.

2.2 Problem formulation

We study the design and sizing of an axially loaded timber member with dowel-type timber joints that represents a braced frame element (column or diagonal) under gravity and wind loads. L is the length and $\eta = h/b$ (where h and b are respectively the height and width of the cross-section) the cross-section aspect ratio of timber element.

We consider a typical configuration of a dowel-type connection with four shear planes with two slotted-in steel plates, as illustrated in **Figure 2**. We choose to design our joint with discontinuous dowels, i.e. with two half-dowels, and a timber thickness distribution of $\frac{1}{4} | \frac{1}{2} | \frac{1}{4}$ (**Figure 2b**). As noted by Bocquet [30] this particular layout allows controlling the load distribution on timber members – as much load is transferred to the central part as to the side parts – and facilitates assembling in particular when the gap in the connection must be minimized. This solution (i.e. half-dowels) has been chosen for the construction of recent buildings such as the “Fondation Louis Vuitton” in Paris, or the “Allianz Riviera Stadium” in Nice. Given this configuration, load-bearing capacity is independent of the thickness of the plate and the following design equations can be applied for calculating the load-bearing capacity $F_{v,Rk}$ and stiffness K_{ser} per shear plane of a half-dowel:

$$F_{v,Rk} = \min \begin{cases} f_{h,1,k} t_1 d & (f) \\ f_{h,1,k} t_1 d \left[\sqrt{2 + \frac{4M_{y,Rk}}{f_{h,1,k} d t_1^2}} - 1 \right] & (g) \\ 2.3 \sqrt{M_{y,Rk} f_{h,1,k} d} & (h) \end{cases} \quad (2-1)$$

$$K_{ser} = 2 \times \rho_m^{1.5} d / 23 \quad (2-2)$$

where $f_{h,1,k}$ is the characteristic embedment strength and ρ_m the mean density of timber, t_1 is the timber side member thickness, d the fastener diameter, $M_{y,Rk}$ its characteristic yield moment. The total characteristic capacity $R_{v,Rk}$ and stiffness $K_{c,U}$ of the connection for the Ultimate Limit State (ULS) with n_{tot} number of dowels can thus be determined from the following equations, considering the equivalent spring model shown in [31]:

$$R_{v,Rk} = \sum_{j=1}^{n_{plate}} \left[n_{plan,j} \times \sum_{i=1}^{n_2} n_{ef,i} F_{v,Rk} \right] \quad (2-3)$$

$$K_{c,U} = 4 \times \frac{K_{w,U,t1} \cdot \frac{2}{3} K_{ser,p}}{K_{w,U,t1} + \frac{2}{3} K_{ser,p}} = 4 \times \frac{K_{w,U,t1} \cdot \frac{2}{3} (n_{tot} K_{ser})}{K_{w,U,t1} + \frac{2}{3} (n_{tot} K_{ser})} \quad (2-4)$$

$$\text{With } K_{w,U,t1} = K_{w,U} t_1 / (\sum_j t_j) = \frac{2E_{0,05}A}{L_c} \times t_1 / (\sum_j t_j) \quad (2-5)$$

where $n_{plate} = 2$ and $n_{plan} = 2$ are respectively the number of steel plates and shear plans per plate, $n_{ef,i}$ is the effective number of fasteners in the i^{th} row, $K_{w,U,t1}$ the local stiffness of timber associated to the thickness t_1 , L_c the length of the connection, E and A the young’s modulus and cross-section area of the timber member. Note that the connection stiffness at Service Limit State (SLS) is taken as $K_c = 3/2 K_{c,U}$

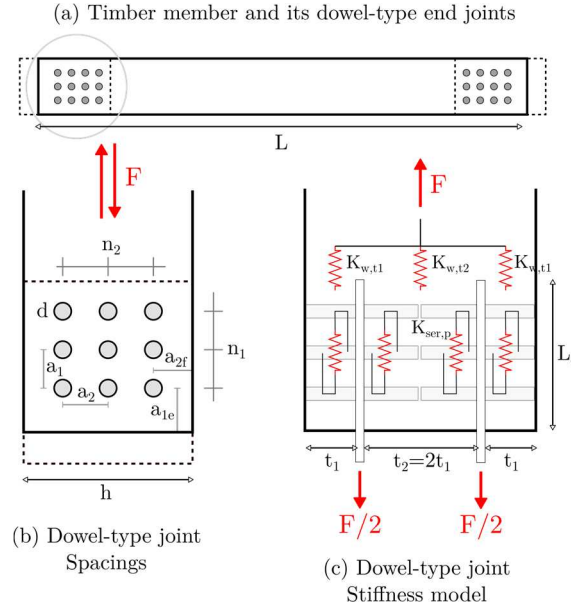


Figure 2 : Geometry and notation of a dowel-type timber joint with two slotted-in plates

Note that the spring model used in this paper for connection stiffness calculation takes into account not only the stiffness of each shear plane of the connection but also the linear behavior of timber in the connection area, as suggested in [31]. Equivalent springs are introduced to model the axial stiffness of outer and inner timber parts. The stiffness of a shear plane $K_{ser,p}$ is obtained by multiplying the stiffness K_{ser} from (2-2) by the total number of fasteners.

In some cases, member sizing can directly be determined by the numbers and geometric characteristics of the connector rather than by the strength requirements of the member material. A compact joint is generally sought by designers to reduce the amount of steel and/or limit the size of the connection compared to that of the timber member. To highlight this design principle, we can define two simple constraints regarding joint dimensions to assess its compactness as illustrated in **Figure 3**:

- The number of column in the connection should not exceed a certain factor α of the number of rows: $n_1 \leq \alpha n_2$
- The length of the connection should not exceed a certain ratio β of a reference length: $L_c \leq \beta L_{ref}$. This reference length is, in general, the length of the timber member, but could also be different. For example, for a column, the floor height could be used.

For connections with rows of fasteners arranged and loaded parallel to the grain, because of the non-uniform load distribution between fasteners, the total load-bearing capacity of the connection is smaller than the sum of single individual strengths. This “group effect” increases as fastener spacing parallel to the grain decreases. To reduce this phenomenon, connections can be reinforced with screws perpendicular to the grain to increase the local strength in shear and tension perpendicular to the grain. In connections with sufficient reinforcement between the dowels, the timber

does not split and the effective number n_{ef} equals the actual number n_{tot} of dowels [32]. The impact of the two configurations (with and without reinforcement) will be analyzed in section 2.4.

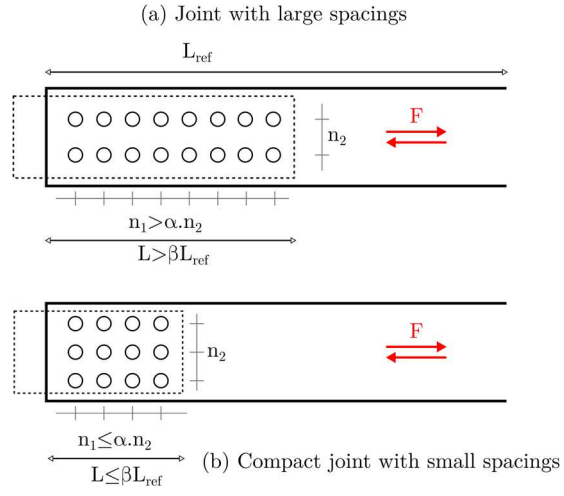


Figure 3 : Compactness of dowelled connection

2.3 Sizing procedure

The timber member is first checked for tensile and compressive strength as well as for buckling criteria, defined in EC5 [22]. The contribution of the local bending moments is neglected.

$$\sigma = F / A \leq \sigma_{t,Rd} = k_{mod} f_{t,0,k} / \gamma_M \tag{2-6}$$

$$\sigma = F / A \leq \sigma_{c,Rd} = k_c k_{mod} f_{t,0,k} / \gamma_M \tag{2-7}$$

For a given axial force F , a cross-section aspect ratio η and a length L , timber member is sized – i.e. the height of the cross-section h is chosen – according to the previous system of equations. From these minimum cross-section dimensions and within a set of fastener spacing and distances in accordance with EC5 [22] specifications, the connection is then sized – i.e. we choose the minimum number of dowels for a given load-bearing capacity. If found to be in violation with joint compactness design principles, the height of the cross-section is increased to add one row of dowels, and the connection sizing process is repeated. Global design procedure is summarized in **Table 1**.

For $F, L, \eta, \alpha, \beta$	
1.	Calculate cross section dimensions $h^{(0)}$ ($\eta b^{(0)} = h^{(0)}$) to satisfy tensile resistance of timber member $\sigma < \sigma_{t,Rd}$
2.	Calculate cross section dimensions $h^{(1)}$ ($\eta b^{(1)} = h^{(1)}$) to satisfy compression resistance of timber member with buckling $\sigma < \sigma_{c,Rd}$
3.	Initialize cross section dimensions for connection design $h^{(2)} = \max(h^{(0)}; h^{(1)})$
4.	WHILE $R_{v,Rd} \leq F$
4.1	Calculate the number of row n_2
	Initialize the number of columns $n_1 = 0$
4.1	WHILE $n_1 < \alpha n_2$ and $L_{ass} \leq \beta L$ and $R_{v,Rd} < F$
	Add one column of dowels: $n_1 = n_1 + 1$
	Calculate efficient number of fasteners: n_{ef}
	Calculate $F_{v,Rd,tot}, L_{ass}$
4.2	IF $R_{v,Rd} < F$
	Update member cross section $h^{(2)}$ to add one row: $n_2 = n_2 + 1$

Table 1 : Sizing procedure of an axially loaded timber element and its dowel-type joint

2.4 Semi-rigid timber connection: strength vs. stiffness

For numerical examples, the following hypotheses are assumed. Steel dowels with a diameter d of 16 mm and steel grade 5.6 with an ultimate tensile strength $f_{u,k}$ equal to 500 MPa are used. Timber member is assumed GL28h glued laminated timber with a square cross-section (i.e. $\eta = 1$). The design load-carrying capacities of the timber member and its connection are calculated by considering a strength modification factor $k_{mod} = 1$ and safety factors $\gamma_M = 1.25$ for timber element and $\gamma_M = 1.3$ for connections. We choose $\alpha = 4$ and $\beta = 0.3$ for connection compactness parameters. The minimum fastener spacing and distances in the connection according to EC5 are used and defined as follows: $a_1 = 5d$ (parallel to grain), $a_2 = 3d$ (perpendicular to grain), $a_{3,t} = \max(7d; 80mm)$ (loaded end), $a_{4,t} = 4d$ (loaded edge). We suppose that the connection is reinforced, so that $n_{ef} = n_{tot}$. The analysis is conducted for an axial force range $F = [1; 2 \times 10^4]$ kN, and the reference length and the buckling length are assumed to be equal.

Example curves of axial stiffness of the connection for the ultimate limit state vs. load carrying capacity for different reference lengths are shown in **Figure 4**. Using a least-squares fitting method, linear regression $K_{c,U} = c_1 F$ and 2nd degree polynomial $K_{c,U} = c_2 F^2 + c_1 F$ regression models are performed on numerical data. The coefficients of these regressions as functions of the member reference length (with and without reinforcement) are shown in **Figure 5**.

Figure 4 illustrates that the stiffness behavior of the dowel-type connection can be approached by a linear function of the axial force in the member. As could be expected, for low values of the reference length L_c , member sizing is mainly controlled by connection design, and the evolution of stiffness is very close to the linear regression model. For higher values of L_c , member sizing is first controlled by compression for small values of the axial force, and then by traction for higher loading.

Figure 5 shows that the slope c_1 of the linear regression model first decreases with the reference length for small L_c , and then converge toward a lower value for high L_c . However, it should be noted that for high values of the reference length, the linear model slightly deviates from the observed behavior (see **Figure 4c**), and we note a concave shape of stiffness vs. axial force curves. This behavior is confirmed by the negative values taken by the quadratic coefficient c_2 of the polynomial regression model (see **Figure 5**) for high L_c values.

The introduction of the local timber behavior through the term K_w in equation (2-4), allows describing an effect of the connection geometry on the overall stiffness. Without this term, joint stiffness would depend only on the number of dowels and shear planes. Thus, the relationship between stiffness and capacity becomes very close to the linear regression model with a slope almost independent of the reference length, as seen in **Figure 6b**. On the contrary, with the spring model shown in **Figure 2** and described by the equations (2-4) and (2-5), a more compact joint – *i.e.* with a shorter connection length L_c – results in a larger apparent stiffness K_w of the wood in the connection area that participates to the load transfer to the fasteners. Hence, the more compact, the larger the connection stiffness $K_{c,U}$ will be according to (2-4). This explains the concavity of stiffness curves for high values of the reference length, because connection design is not constrained by compactness requirements, and L_c freely increases with loading.

For intermediate reference length (see **Figure 4b**), the concave behavior previously described is observed until a threshold loading value above which compactness requirements start to control member sizing – no new column of dowels can be added without violating compactness criteria – and stiffness increases linearly.

As expected, within the proposed framework, **Figure 5b** shows that without reinforcement, more dowels are needed to achieve the same load-carrying capacity. As the number of dowels is more important without reinforcement, the stiffness of the connection is higher. Indeed, according to the EC5 approach, no group effect should be considered for stiffness calculation of multiple fastener connections. Moreover, reinforcements are not supposed to have any influence on the stiffness of individual connectors.

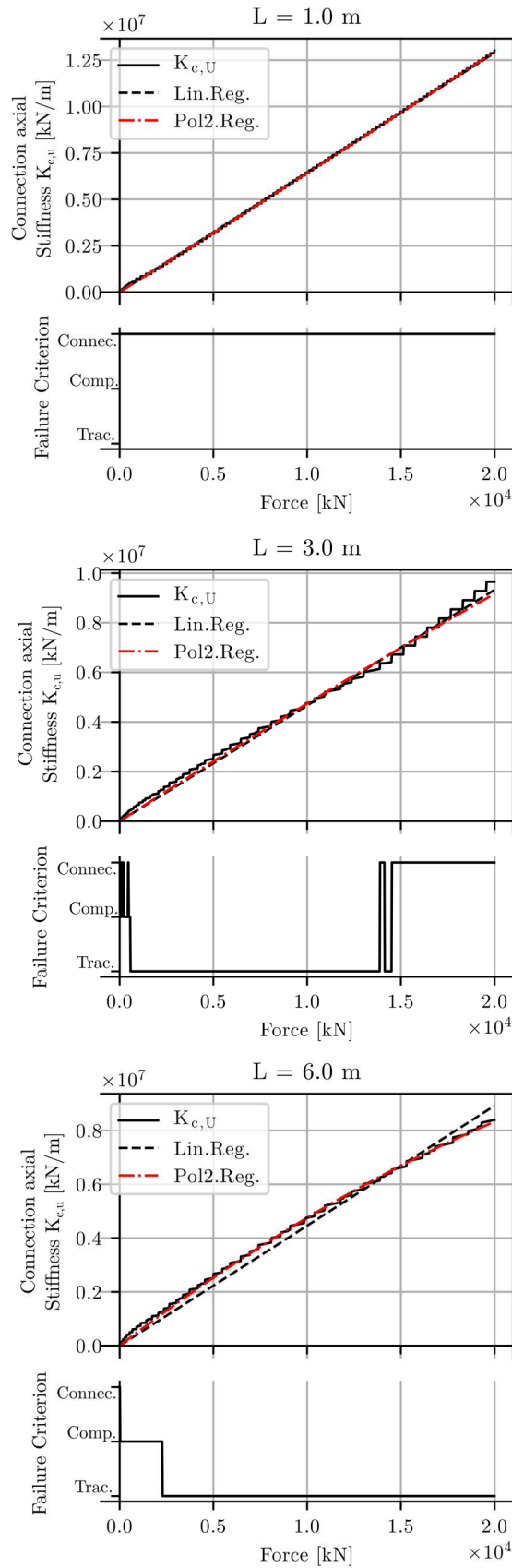


Figure 4 : Sizing of an axially loaded timber member and its dowel-type connection for $L = 1, 3$ m and 6 m
 (Top) Plot of the connection stiffness (at ultimate limit state) versus axial carrying capacity of the member + joint
 (Bottom) Member failure criterion versus axial carrying capacity (Conne. = connection, Comp. = compression, Trac.. = traction)

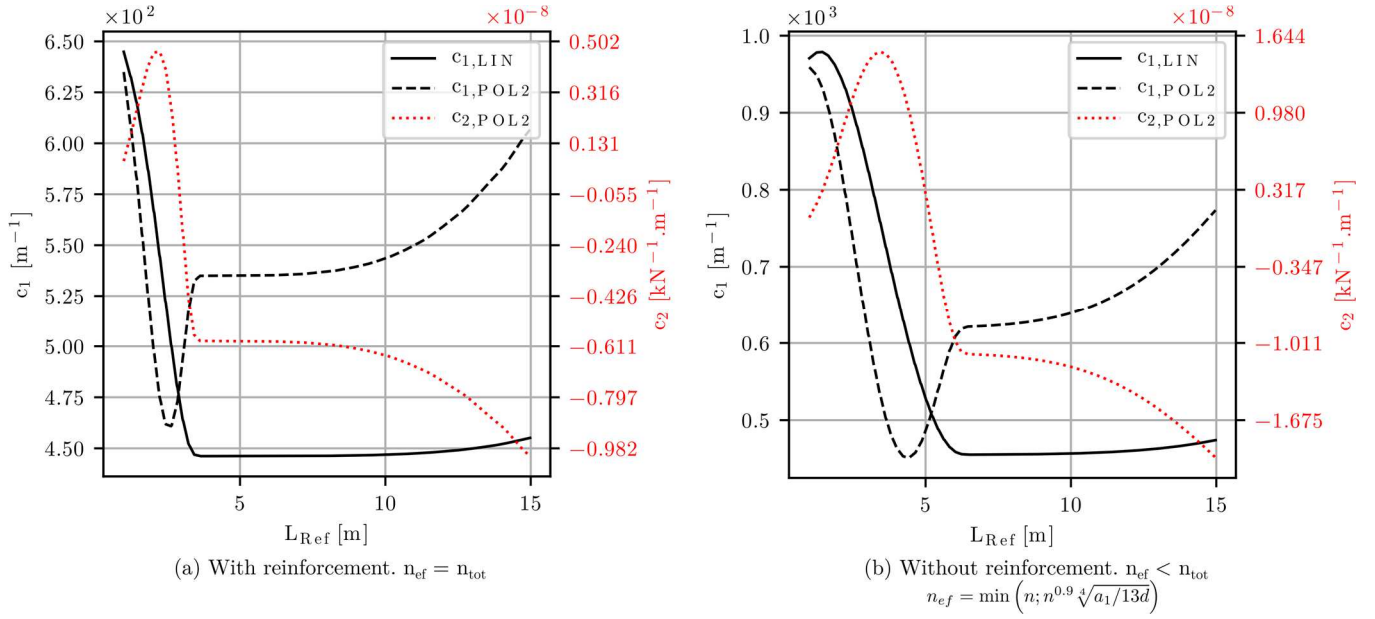


Figure 5 : Stiffness behavior of an axially loaded dowel type connection at ultimate state. Linear regression $K_{c,U} = c_1 F$ and polynomial regression $K_{c,U} = c_2 F^2 + c_1 F$ coefficients versus reference length with and without reinforcement

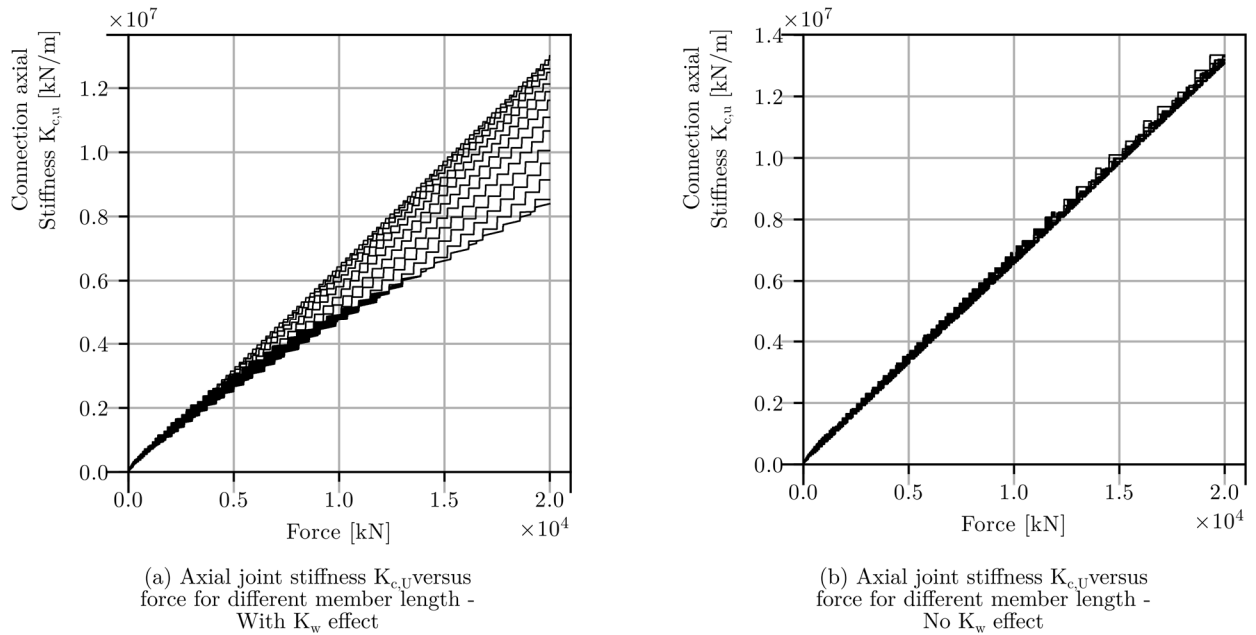


Figure 6 : Axial joint stiffness $K_{c,U}$ versus load carrying capacity of the timber member and connections for different reference member length.

3. Braced frame problem and shape optimization methodology

3.1 Braced frame optimization problem

We study the optimal geometry – and sizing – of a braced frame structure part of the lateral system of a high-rise building subject to wind loading shown in **Figure 7** and previously described by Stromberg *et al.* [10]. The frame has an overall height H and a half-width B and is composed of N bracing modules along the height. The top-height of the n^{th}

bracing module is given as z_{2n} and the height of the intersection of the diagonals as z_{2n-1} . No horizontal beam connecting both columns is considered. Each timber member is supposed to have a square cross-section A_i and dowel-type joints at both end **Figure 7c**. Node locations z and cross-sectional area A_i are the design variables of the shape + size optimization problem.

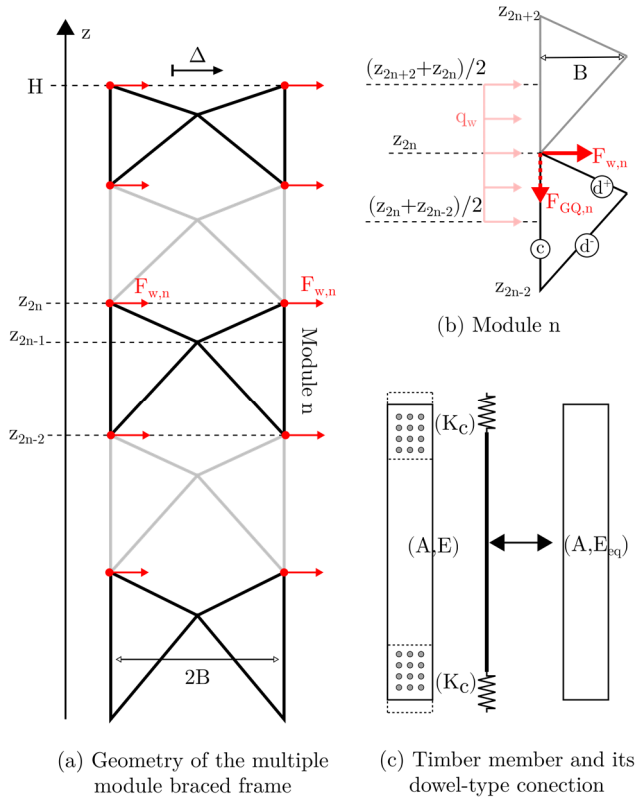


Figure 7 : Geometry and notation of the multiple modules braced frame optimization problem.

In lateral system design for high-rise structures, multiple structural objectives can be considered, mainly, overall drift, compliance, period and buckling. Each objective relates to a different aspect of the design, but they all can affect the topological layout of the structural system and the sizing of the members. In the present work, the structure is subject to an overall drift constraint under wind load, with a limit of displacement at the top of the structure set to $H/500$. Depending on the model, strength requirements – for ultimate limit state load combinations – is considered, in order to study the impact on member sizing and optimal layout of the frame.

Wind load profiles are generally modeled by a power or logarithmic law, describing the increase of wind velocity with height. However, not to introduce unnecessary complexity, a uniform wind load distribution q_w is used. As illustrated in **Figure 7b**, wind load is distributed to the nodes of the frame, with equivalent lateral forces acting at the top of each module $F_{W,n}$.

This truss structure is statically determinate. By applying a unit horizontal load at the top of the j^{th} module on both sides, internal forces in the top $f_{n,d+}^j$ and bottom $f_{n,d-}^j$ diagonal members and in the column $f_{n,c}^j$ of the n^{th} module are given by the following equations:

$$\begin{aligned} f_{n,c}^j &= \frac{(z_{2n} - z_{2n-1})}{B} \\ f_{n,d+}^j &= \frac{L_{n,d+}}{B} = \frac{\sqrt{(z_{2n} - z_{2n-1}) + B^2}}{B} \\ f_{n,d-}^j &= \frac{L_{n,d-}}{B} = \frac{\sqrt{(z_{2n-1} - z_{2n-2}) + B^2}}{B} \end{aligned} \quad (3-1)$$

Using the Principle of Virtual Work (PVW), the displacement Δ_k^j at the top of the k^{th} module under a unit load at the top of the j^{th} module on both sides is

$$\Delta_k^j = 2 \sum_{n=1}^{n \leq j} \left[\sum_{m=[c,d+,d-]} f_{n,m}^j f_{n,m}^k \left(\frac{L_{n,m}}{(EA)_{n,m}} + \frac{2}{K_{c,n,m}} \right) \right] \quad (3-2)$$

where $A_{n,m}$ is the cross-sectional area of a member, $L_{n,m}$ its length and $K_{c,n,m}$ the stiffness of the end dowel-type joints. Note that in the following, for sake of simplicity and generalization, the numbering of members is changed from $(n, m) \in ([1: N][c, d^-, d^+])$ to just i being the index of the elements.

We finally define distributed gravity loadings q_G and q_Q acting only on vertical elements, which accounts for the portion of dead (G) and live loads (Q) applied on the floors of the building and transferred to the columns of the frame.

3.2 Member sizing: Optimality criteria

For a given geometry, the sizing optimization processes developed here seeks to achieve the minimum weight solution of the frame structure under both strength and top-displacement constraints. The cross-sectional dimensions A_i assigned at each element are the design variables of this problem.

Numerous methods have been developed to solve the member sizing optimization problem previously stated. In the late '60s, *Optimality Criteria* (OC) methods for structural optimization were introduced. These methods originally mirror the manual and intuitive design process of engineers, but in an automated and more consistent manner. OC methods are based on the statement of an a priori optimal criterion and a resizing algorithm to attempt to reach this criterion.

The famous *Fully Stressed Design* (FSD) [33] technique was the starting point of OC development. FSD is based on the intuition – previously introduced by Maxwell [34] and Michell [35] – that in an optimal structure each member is

subjected to its allowable stress under at least one of the loading conditions. FSD methods have proven their efficiency for many problems involving determinate – or not too statically indeterminate – structures subject to strength requirements.

The success of FSD prompted extensions to optimization under stiffness constraints with strain energy criterion [36,37], which became the basis of modern rigorous OC methods based on the Karush-Kuhn-Tucker (KKT) conditions of optimality that are solved iteratively [38,39]. Chan *et al.* [40,41] present an approach tailored to the design of the lateral system of tall buildings, subject to drift and strength constraints.

Although the serviceability drift requirements mainly control the design of the lateral systems of a tall building, the strength and stability of their members should also be verified to ensure the structural safety of the building. There are two main approaches to member sizing with respect to both local strength/stability requirements, and global drift constraints [40]. They can both be considered explicitly in terms of design variable and treated in the same optimization process. On the other hand, they can be dealt with separately, and be implicitly accounted for in the other's process. More specifically here, as stiffness generally controls the design of bracing systems, member's strength and stability can be treated as secondary constraints since most of them will not be finally active. Thereby, once the structure is analyzed and the strength-based member sizes are determined, they can be used as the lower-size bounds on the design variables for the optimization of the structure's stiffness.

3.3 Connection sizing

The behavior of axially loaded dowel-type joints has been studied in section 2. It has been found that, on initial examination for design stage, the relationship between stiffness and load-bearing capacity can be modeled by a linear regression model. Numerical results from section 2.4 are used. The stiffness of a connection depends on:

- $F_{Rd,i}$ – Design tensile/compressive force. As the analysis presented in section 2 was conducted using a modification factor for the duration of load and moisture content $k_{mod} = 1$, design forces calculation takes into account the modification factor k_{mod} of each ULS load combinations using the equation (3-3).
- c_1 – The slope of the linear regression model, which, as noted in section 2, can depend on the reference length L_{ref} considered for joint compactness criteria. We suppose here that c_1 is constant for all timber members, regardless of their length. However, the sensitivity of the results with respect to this parameter will be analyzed in section 4.

$$K_{c,U,i} = c_1 \times \max_{ULS} [F_{Rd,i}/k_{mod}] \quad (3-3)$$

Note that we assume here that wind loads, as well as gravity loads, are transferred through the dowel-type joints.

3.4 Overall design and optimization process

The overall optimization process is solved by a two-level optimization routine: at a low-level, for a fixed geometry, size optimization techniques are used to find the optimal material distribution in the frame given the strength and drift requirements. Then a more general optimization method is used to solve the global shape optimization problem of the timber frame (see **Figure 8**).

- (A1) For a given geometry of the frame, internal forces in members are first calculated for wind (W), dead (G) and live (Q) loads. In accordance with the previously described methodology, the stiffness of end joints $K_{c,U,i}$ is then estimated.
- (A2) A classic FSD technique with a stress-ratio resizing rule is used to obtain the minimum sizing of each member A_i^{FSD} of the frame under ULS load combinations to satisfy EC5 strength requirements. For buckling length calculations, we suppose that members are stabilized at each floor.
- (A3) Sizing optimization for top-displacement constraint under wind load is then performed using a rigorously derived OC method as presented in [41]. The previously calculated strength-based cross-sectional area A_i^{FSD} act as lower size bounds on the design variables.
- (B) Finally, the global shape optimization problem to minimize the volume of timber material is solved using a *Constrained Optimization by Linear Approximation* (COBYLA). COBYLA is a derivative-free algorithm that constructs successive linear approximations of the objective and constraint functions by interpolation at the vertices of a simplex and optimizes these approximations in a trust region at each step [42].

The overall design and optimization process is summarized in **Figure 8** and has been implemented in SciPy [43], a Python based ecosystem. More details of each step are provided in the following sections.

Note that in the proposed framework, the structure is supposed to be statically determinate. In the case of statically indeterminate structures, after each design cycle for size optimization (A), the structure could be reanalysed with the updated cross-section, and the design process would be repeated until convergence.

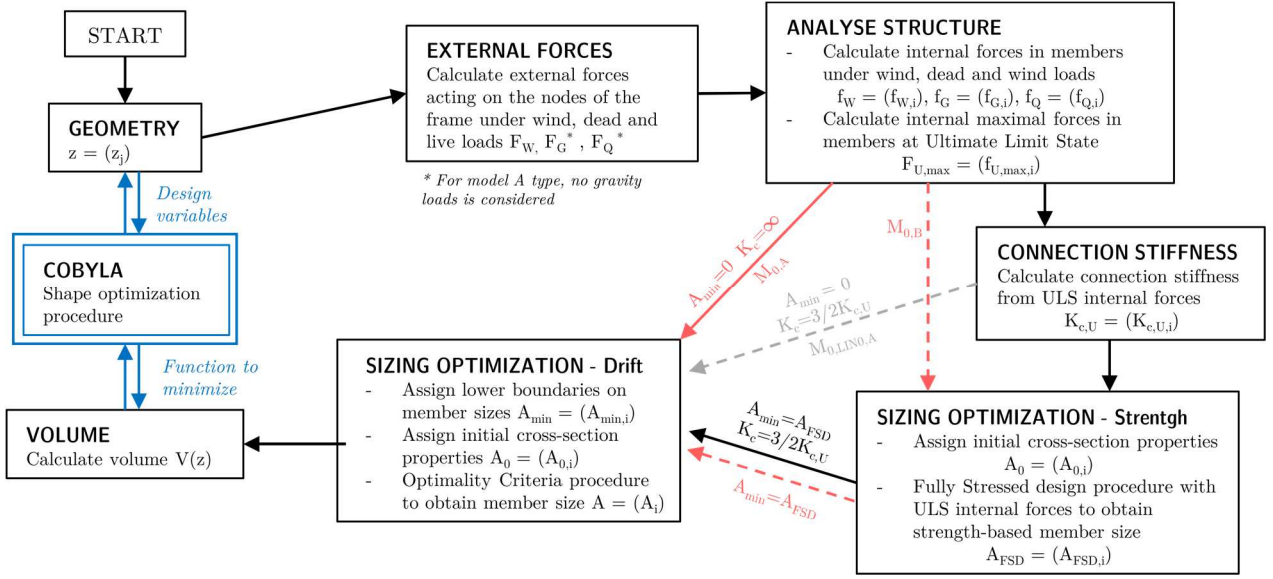


Figure 8 : Optimization process.

3.4.1 Sizing for strength constraints

To implement the FSD approach, a stress-ratio resizing rule is used

$$A_i^{(v+1)} = A_i^{(v)} \left(\max_{ULS} \frac{\sigma_i^{(v)}}{\sigma_i^U} \right)^\eta \quad (3-4)$$

$$\text{With } \sigma_i^U = \min (k_c k_{mod} f_{c,0,k} / \gamma_M ; k_{mod} f_{t,0,k} / \gamma_M)$$

Where v and $(v + 1)$ indicate two successive iterations and η is a relaxation factor used to improve the rate of convergence. According to (3-4), a member is designed to satisfy its most critical stress state under the worst loading conditions.

3.4.2 Sizing for displacement constraint

The design optimization problem involving explicit drift and implicit sizing constraints can be stated as follows:

$$\min_{A_i} V = \sum_i A_i L_i$$

Subject to :

$$\Delta_N = \sum_i F_i f_i^N \left(\frac{L_i}{(EA)_i} + \frac{2}{K_{c,i}} \right) \leq \frac{H}{500} \quad (3-5)$$

$$A_i^{min} = A_i^{FSD} \leq A_i$$

The Lagrangian function of the problem (3-5) is

$$L(A_i, \lambda, \mu_i) = \sum_i A_i L_i + \lambda \left[\sum_i \left(F_i f_i^N \left(\frac{L_i}{(EA)_i} + \frac{2}{K_{c,i}} \right) \right) - \Delta_{lim} \right] + \sum_i \mu_i (A_i - A_i^{min}) \quad (3-6)$$

The Karush-Kuhn-Tucker conditions of optimality for this problem lead to

$$\frac{\partial L}{\partial A_i} = 0 \Rightarrow \lambda \left(\frac{F_i f_i^N}{E} \times \frac{1}{A_i^2} \right) + \mu_i / L_i = 1 \quad \forall i \quad (3-7)$$

$$\lambda \frac{\partial L}{\partial \lambda} = 0 \Rightarrow 2 \sum_i \left(F_i f_i^N \left(\frac{L_i}{(EA)_i} + \frac{2}{K_{c,i}} \right) \right) = \Delta_{lim} \text{ or } \lambda = 0 \quad (3-8)$$

$$\mu_i \frac{\partial L}{\partial \mu_i} = 0 \Rightarrow A_i = A_i^{min} \text{ or } \mu_i = 0 \quad (3-9)$$

Equations (3-7), (3-8) and (3-9) represent the optimality criteria that must be satisfied at the optimum. The set of equations can be used to set a recurrence relation for a resizing iterative algorithm over the design variables A_i .

We define ν and $(\nu + 1)$ two successive iterations. At the ν th iteration, we introduce two sets of elements: $B_i^{(\nu)}$ – the set of all inactive elements for which $A_i = A_i^{min}$ and $B_A^{(\nu)}$ – the set of all active elements for which $A_i > A_i^{min}$. For active sizing variables, equation (3-9) implies that $\mu_i = 0$, and we can define a recursive relation similar to the stress-ratio rule for achieving a fully stressed design

$$A_i^{(\nu+1)} = A_i^{(\nu)} \left[\lambda \left(\frac{F_i f_i^N}{E} \times \frac{1}{A_i^{(\nu)2}} \right) \right]^{1/\tilde{\eta}} \quad (3-10)$$

where $\tilde{\eta}$ is a relaxation parameter that controls the convergence rate of the recursive process. Using equation (3-7), and applying a first-order binomial expansion we obtain

$$A_i^{(\nu+1)} = A_i^{(\nu)} \left[1 + \frac{1}{\tilde{\eta}} \left[\lambda \left(\frac{F_i f_i^N}{E} \times \frac{1}{A_i^{(\nu)2}} \right) + \mu_i / L_i - 1 \right] \right] \quad (3-11)$$

Before using the previous recursive relations, the unknown Lagrange multiplier λ must be determined. To establish the current λ value, consider the change – i.e. the differential – $(\Delta^{(\nu+1)} - \Delta^{(\nu)})$ in the drift constraint due to the changes in the active design variables.

$$\Delta^{(\nu+1)} - \Delta^{(\nu)} = \sum_{i \in B_A} \left(\frac{\partial \Delta}{\partial A_i} \right) \Big|_{(\nu)} (A_i^{(\nu+1)} - A_i^{(\nu)}) \quad (3-12)$$

We suppose that the design is controlled by the displacement constraint, so that at the optimum $\Delta = \Delta_{lim}$. We suppose that drift constraint becomes active after the $(\nu + 1)$ th iteration so that $\Delta^{(\nu+1)} = \Delta_{lim}$. Differentiating the displacement with respect to A_i , then substituting with (3-11) into (3-12), terms are rearranged to obtain

$$\lambda^{(\nu)} \times \sum_i \frac{A_i}{\tilde{\eta}} \left(\frac{F_i f_i^N L_i}{EA_i^2} \right)^2 \Bigg|_{(\nu)} = \Delta_{lim} - \Delta^\nu + \sum_i \frac{A_i}{\tilde{\eta}} \left(\frac{F_i f_i^N L_i}{EA_i^2} \right) \Bigg|_{(\nu)} \quad (3-13)$$

Having the current set of design variables $A_i^{(\nu)}$, the corresponding value for the Lagrange multiplier $\lambda^{(\nu)}$ is determined by solving equation (3-13). Finally, the new set of variables $A_i^{(\nu+1)}$ is found with the recursive relation (3-10). During the iterations, some members may be found to exceed their limiting sizes. Once a sizing variable reaches a limiting value, it is not allowed to change any further and the set of active B_A and inactive B_I members are updated for the next iteration.

4. Results: influence of semi-rigid connections

To assess the impact of connection stiffness and strength requirements on the optimization of a braced frame for top drift constraint, various models are studied and presented in **Table 2**. In models "A", no gravity loads and no strength requirements are considered for member sizing. In models "B", gravity loads are introduced and strength requirements at ULS are taken into account for member sizing optimization. "0" indicates that the stiffness of timber joints are not considered, while "K" indicates that the semi-rigid behavior is included in the frame analysis. "LIN" indicates that the simplified linear relation for timber connection stiffness (3-3) is used.

Load combinations and modification factor considered under ULS design are presented as follows, where G, W, and Q are dead load, wind load, and live load respectively:

$$\begin{aligned} ULS0 &= (1.35G, k_{mod} = 0.6) = ULS.G \\ ULS1 &= (1.35G + 1.5Q, k_{mod} = 0.8) = ULS.GQ \\ ULS2 &= (1.35G + 1.5W + 1.05Q, k_{mod} = 1.1) = ULS.GWQ \end{aligned} \quad (4-1)$$

Model	Connection Stiffness*	Member Sizing	Gravity loads
M _{0,A}	$K_{c,U,i} = \infty$	Overall Stiffness Optimization	No
M _{K,LIN,0,A}	$K_{c,U,i} = c_1 F_{U,i}$ **		
M _{0,B}	$K_{c,U,i} = \infty$	Overall Stiffness Optimization + ULS(G+GQ+GWQ)	Yes
M _{K,LIN,0,B}	$K_{c,U,i} = c_1 F_{U,i}$ **	strength	

* $K_{U,i}$ indicates the connection stiffness at ULS and is calculated from ULS internal forces in members $F_{U,i}$. Connection stiffness at SLS is given by the relation $K_{c,i} = 3/2 K_{c,U,i}$

** $F_{U,i} = \max_{ULS} [F_{R,d,i} / k_{mod}]$

Table 2 : Notation and description of the different models used for the optimization of the braced frame. Influence of connection stiffness and member sizing criteria.

4.1 Single module frame

The analysis is first conducted for a single module braced frame subject to a point load at the top, as shown in **Figure 9**. As analytically and numerically described by Stromberg *et al.* [10], without any consideration of joint stiffness, strength requirements and gravity loads, the optimal geometry of the single module – i.e. that minimizes the tip deflection of the frame – is defined by a height ratio z/H of 0.75.

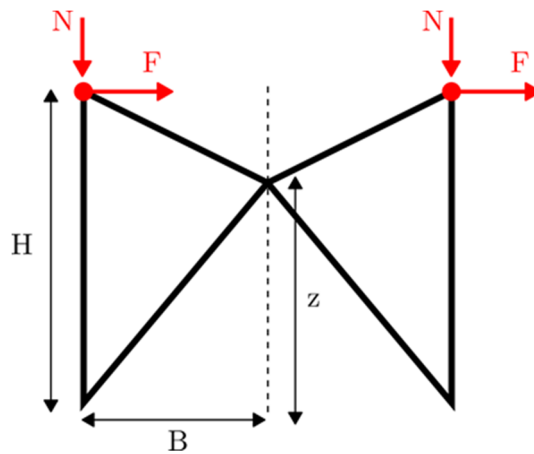


Figure 9 : Single module frame stiffness optimization problem

For the following numerical example, we assume that $c_1 = 0.65 \text{ m}^{-1}$ and that drift constraint is set to $H/500$. **Figure 10** shows the optimal brace work point as a function of the aspect ratio H/B , for different values of the frame's half-width B . For model $M_{0,A}$, the results confirm that the optimal bracing work point for minimal tip deflection is located at 75% of the height of the module regardless of the aspect ratio. According to the figure, for high and medium values of the aspect ratio ($H/B > 2$), the optimum geometry for model $M_{K,LIN0,A}$ depends very little on the aspect ratio of the frame. It can be noted that the connection stiffness leads to a marginal increase in optimum work point ratio, which becomes almost negligible as width increases. We also notice that for aspect ratio under 2 (*i.e.* when the height of the module is lower than its width), the optimal intersection of the cross-brace significantly moves upward.

As expected and shown in **Figure 11**, the loss of stiffness due to doweled connections in model $M_{K,LIN0,A}$ is compensated by members with larger cross-section, leading to a greater volume of timber used in the frame than in model $M_{0,A}$.

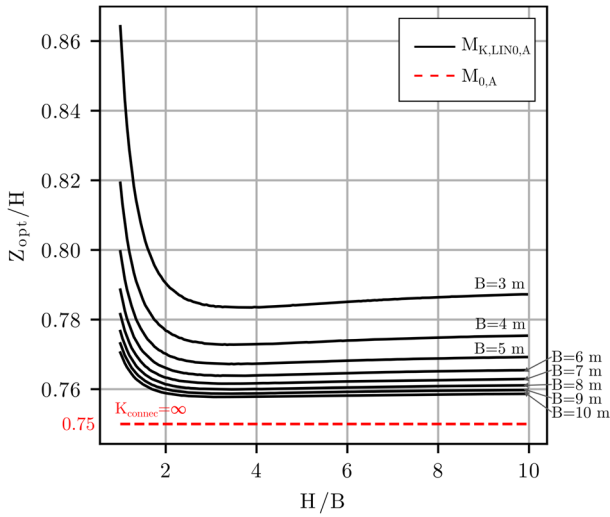


Figure 10 : Single module frame stiffness optimization under wind load only (Models A). Brace work point z/H vs. aspect ratio H/B for different values of frame half-width B

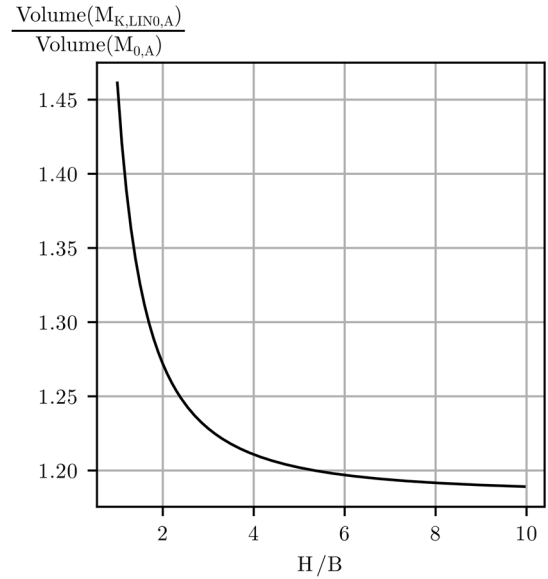


Figure 11 : Single module frame stiffness optimization under wind load only (Models A). Volume ratio between model $M_{0,A}$ and $M_{K,LIN0,A}$ as a function of the module aspect ratio

Strength requirements on members could influence this optimum, and particularly as columns are generally to be sized for gravity loads. This impact is assessed by introducing a dead load N applied to the columns (see **Figure 9**), and by considering strength requirements under the different ULS load combinations. **Figure 12** shows the optimum geometry (z_{opt}/H) versus ($N/(FH/B)$) which represents a ratio between an indicator of the axial force in the columns due to bending under the horizontal load F , and the axial force caused by the gravity load N . Results are calculated for $B = 6\text{ m}$ and different values of the aspect ratio H/B . For small values of the ($N/(FH/B)$) ratio the optimum work point ratio remains close to 0.75 (strictly equal for model $M_{0,A}$), as the design of the frame, and particularly column sizing, is controlled by lateral drift requirements. Above a certain threshold value of ($N/(FH/B)$) ratio, a significant change of behavior is observed, and the optimum work point significantly moves down. Strength requirements start to control columns sizing. Therefore, the column area is higher than the optimal area. As strength-based size increases with N , the bending rigidity of the frame increases and the displacement becomes mainly due to axial deformation of the diagonals, in other words, due to shear deformation of the frame. For very large values of ($N/(FH/B)$) ratio, the problem can be reduced to a pure-shear beam problem in which the optimum intersection of the cross-brace is located at 50% of the module height.

As might be expected, introducing semi-rigid connections results in a slightly higher breakpoint in model $M_{K,LIN0,B}$ than in $M_{0,B}$. Finally, it should be noted from **Figure 12** that, in the same way, the larger the aspect ratio H/B , the larger the range in which design is controlled by stiffness is extended.

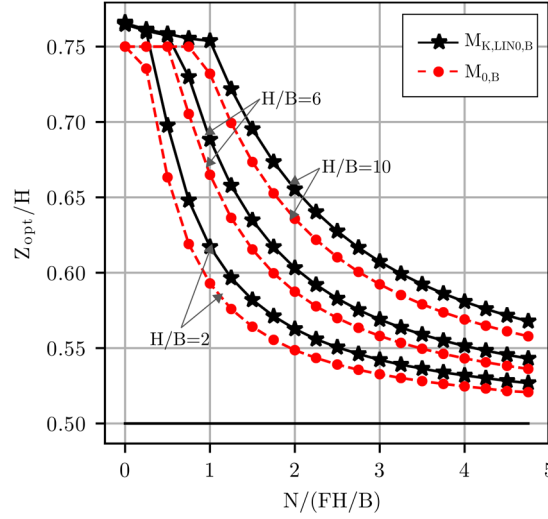


Figure 12 : Single module frame stiffness optimization with strength constraints under gravity and wind loads (Models B). Brace work point z/H vs. aspect ratio $N/(FH/B)$ for different values of frame aspect ratio H/B with $B = 6$ m

4.2 Multiple modules frame

The analysis is now generalized to a braced frame with multiple modules and multiple point loads along the height, as previously described in Section 3. The following parameters are used to illustrate a typical high-rise case study: the height is $H = 80$ m, the width $2B = 12$ m, the number of floors $N_{floor} = 25$, the wind load distribution $q_w = 10$ kN/m, the axial forces per floor in the column due to dead loads $F_{floor,G} = 60$ kN, and due to live loads $F_{floor,Q} = 22.5$ kN. We assume for the stiffness behavior model that $c_1 = 6.5 \times 10^2$ m⁻¹ (model $M_{K,LIN0,B}$) in equation (3-3). The sensitivity of the results with respect to this parameter is conducted assuming $c_1 = 1.0 \times 10^3$ m⁻¹ for model $M_{K,LIN1,B}$ and $c_1 = 4.5 \times 10^2$ m⁻¹ for model $M_{K,LIN2,B}$.

The results of the shape optimization problem for the different models with a varying number of modules are illustrated in **Figure 14**. **Figure 13** shows the associated plot of volume versus the number of modules. A detailed analysis of the solutions for the 4 and 5 modules cases and models $M_{0,A}$ and $M_{K,LIN0,B}$ is presented in **Figure 15**. For each solution, this figure shows: the displacement due to each module, each element type (columns or diagonals) and connections; the utilization ratio of the members for the ULS load combinations described in equation (4-1); and the equivalent Young's modulus ratio E_{eq}/E defined as follows:

$$E_{eq,i}/E = \frac{1}{1 + 2 \frac{EA_i}{K_{c,i}L_i}} \quad (4-2)$$

The loss of stiffness due to doweled connections can be approached by considering an equivalent Young's modulus E_{eq} for each timber member as illustrated in **Figure 7c**.

4.2.1 Volume of timber

As already noted in the single module case, considering connection stiffness leads to a significant increase in the volume of the optimal timber frame compared to model $M_{0,A}$ (see **Figure 13**). **Figure 15** illustrates that the ratio of tip displacement due to the semi-rigid behavior of timber connections is indeed far from being negligible.

It can be noted that this increase of volume, is all the more important as the slope c_1 of the linear model for connection stiffness is low. For example, with a 5 modules frame, for $c_1 = 1.0 \times 10^3 \text{ m}^{-1}$ (model $M_{K,LIN1,B}$), $c_1 = 6.5 \times 10^2 \text{ m}^{-1}$ (model $M_{K,LIN0,B}$) and $c_1 = 4.5 \times 10^2 \text{ m}^{-1}$ (model $M_{K,LIN2,B}$), the volume of timber increases respectively by 25%, 43%, and 72% compared with the model without semi-rigid joints. Moreover, the introduction of connection stiffness behavior can have a direct influence on the optimal topology of the frame (**Figure 13** and **Table 3**). Without joints (models $M_{0,A}$, $M_{0,B}$) or with stiff ones ($M_{K,LIN1,B}$), the optimal number of modules is 5, whereas, in the case of more flexible connections, the optimal number of modules is 4.

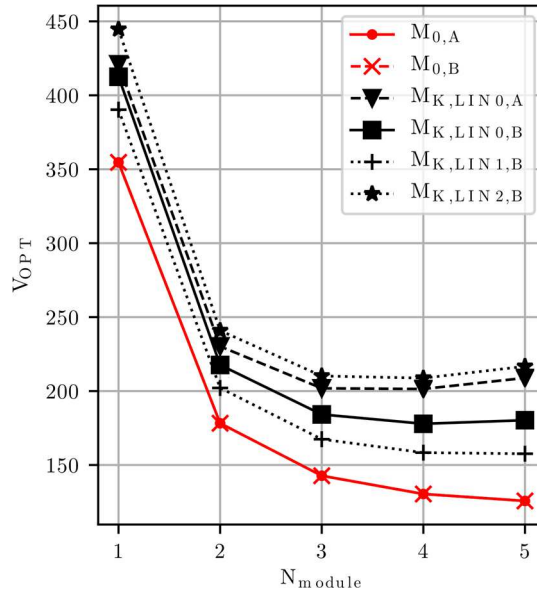


Figure 13 : Plot of volume versus number of modules.

4.2.2 Optimum geometry

From a geometric point of view, overall, connection stiffness has little effect on the relative work point ratio of each module (height of the intersection of the diagonals on the total height of the module) and remains close to 0.75, which generalizes the observation already made for the single module problem. However, two exceptions are worth mentioning and will be analyzed in the next paragraphs.

The main difference introduced by connection semi-rigid behavior in optimal solutions lies in the distribution of modules along the height. For model $M_{0,A}$, modules are equally distributed in height, and the optimal bracing point ratio is 0.75. Looking at the detailed analysis of $M_{0,A}$ solutions in **Figure 15**, we note that the portion of tip displacement due

to each module decrease along the height. Therefore, we can assume that the most efficient way to increase the overall stiffness of a multiple module frame structure is to increase the relative stiffness of the lower modules.

When connection stiffness behavior is taken into account, the optimum distribution deviates from the equally distributed solutions, and modules height consecutively decreases (**Figure 14**). This unequal distribution is more pronounced as the coefficient c_1 of the linear stiffness regression model decreases. Optimal solutions tend to maximize the equivalent Young's modulus ratio E_{eq}/E of timber members defined in equation (4-2), and in particular those of columns, as they account here for the major part of tip displacement (see **Figure 15**). According to equation (4-2), for a given cross-sectional area, the equivalent Young's modulus ratio is higher as the length of the member increases. This observation, combined with the one previously made on the interest to maximize the stiffness of the lower modules, explains the observed distribution for the model with connection stiffness.

Note that this behavior leads to top modules with low aspect-ratio. If the aspect ratio falls under a certain threshold value (more or less under the square aspect ratio), the single module analysis has shown that the optimum work point rapidly moves upwards as aspect ratio decreases. This explains why for model $M_{K,LIN0,A}$ and $N = 5$ (see **Figure 14**), the top module presents a K bracing shape.

4.2.3 Influence of strength requirements

In this example, design and especially member sizing is controlled by overall stiffness. Looking at utilization ratio, **Figure 15**, confirms that, overall, timber members are under-stressed, except maybe for the columns of the higher module. In particular, in the case $N = 5$, the cross-sectional area of higher columns is controlled by strength requirements at ULS. With regards to the influence of strength requirements on optimal geometry observed in the single module frame (see **Figure 12**), the work point ratio of these modules is lower than 0.75, especially for model $M_{K,LIN0,B}$ for which the aspect ratio of the higher module is relatively small.

4.2.4 Convergence and robustness of the optimization process

Note that different initial designs were considered to ensure that the COBYLA algorithm is not stuck in local optima. **Figure 16** shows the various initial designs tested: modules equally distributed along the height with X (**Figure 16a**) and K (**Figure 16b**) bracing, and random module distribution and bracing shape. For all these initial designs, the optimization algorithm converges towards the same geometry, demonstrating the robustness of optimal solutions shown in **Figure 14**.

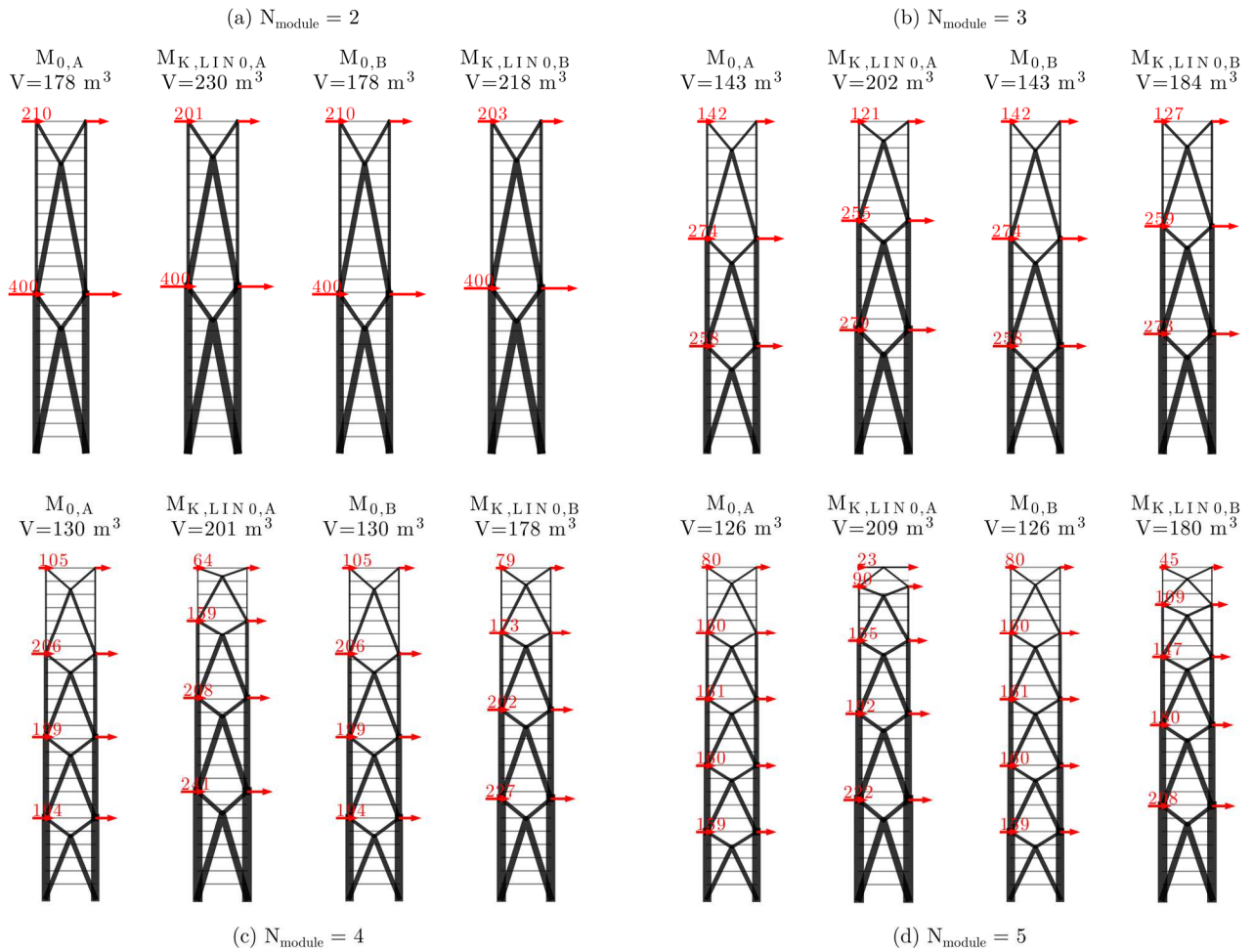


Figure 14 : Shape optimization of a braced frame with multiple modules along the height. Comparison of optimum geometry and volume for the different models. Influence of strength requirements and joint stiffness. NB: cross-sectional areas are relative; light-grey horizontal lines indicates the position of building floors.

Finally, it is worth mentioning that according to **Figure 13**, for models $M_{K,LIN 0,A}$, $M_{K,LIN 0,B}$ and $M_{K,LIN 2,A}$, optimum solutions for $N = 5$ show a volume more important than in the case $N = 4$. This observation highlights the fact that in these cases, the solutions correspond to a local optimum. At first glance, the algorithm is not prevented to converge towards a solution with a lower number of modules (*i.e.* with a module of zero height). However, some penalty functions have been used to enforce strictly positive member length, and as constraints may not be strictly enforced by the COBYLA algorithm used here (*i.e.* small violation is allowed), this might explain why the algorithm has difficulties converging towards solutions with zero-length members. Moreover, in the example above, the optimization process does not converge for a number of modules $N \geq 6$.

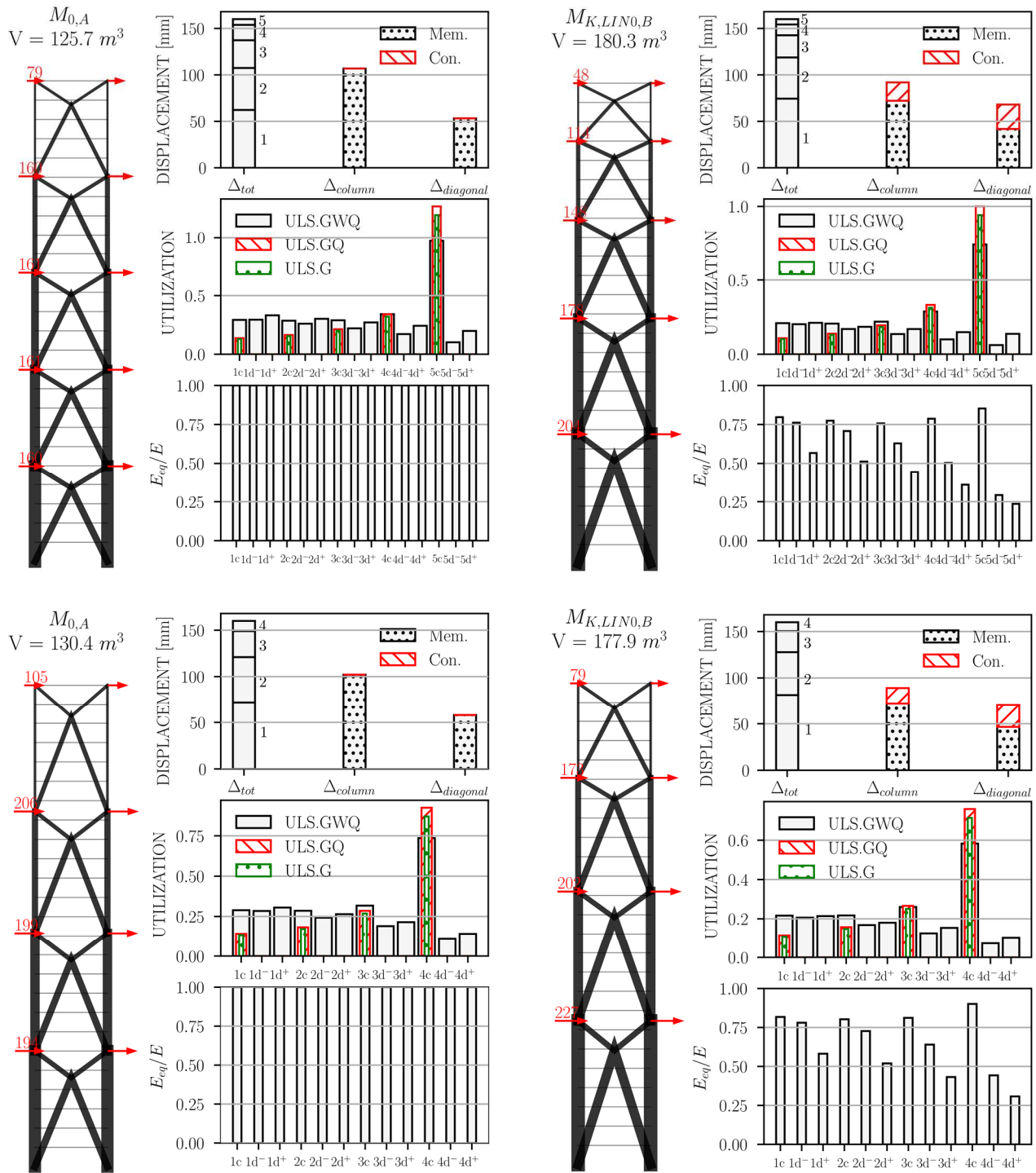


Figure 15 : Shape optimization of a braced frame with 4 and 5 modules. Analysis of optimum geometry and sizing for models M0,A and MK,LIN0,B. NB: cross-sectional areas are relative; light-grey horizontal lines indicates the position of building floors.

Model	N	Volume [m ³]	Module Height [m]					Working Point Ratio				
			1	2	3	4	5	1	2	3	4	5
M _{0,A}	1	354,6	80	-	-	-	-	0,75	-	-	-	-
M _{0,B}	1	354,6	80	-	-	-	-	0,75	-	-	-	-
M _{K,LIN0,A}	1	421,0	80	-	-	-	-	0,77	-	-	-	-
M _{K,LIN0,B}	1	412,5	80	-	-	-	-	0,76	-	-	-	-
M _{K,LIN1,B}	1	390,3	80	-	-	-	-	0,76	-	-	-	-
M _{K,LIN2,B}	1	444,6	80	-	-	-	-	0,77	-	-	-	-
M _{0,A}	2	178,2	38,0	42,0	-	-	-	0,77	0,75	-	-	-
M _{0,B}	2	178,2	38,0	42,0	-	-	-	0,77	0,75	-	-	-
M _{K,LIN0,A}	2	230,2	39,8	40,2	-	-	-	0,79	0,78	-	-	-
M _{K,LIN0,B}	2	217,6	39,4	40,6	-	-	-	0,79	0,76	-	-	-
M _{K,LIN1,B}	2	202,1	38,9	41,1	-	-	-	0,78	0,76	-	-	-
M _{K,LIN2,B}	2	241,0	40,2	39,8	-	-	-	0,8	0,77	-	-	-
M _{0,A}	3	142,7	25,2	26,3	28,5	-	-	0,77	0,77	0,75	-	-
M _{0,B}	3	142,7	25,2	26,3	28,5	-	-	0,77	0,77	0,75	-	-
M _{K,LIN0,A}	3	201,9	29,0	26,9	24,1	-	-	0,79	0,80	0,80	-	-
M _{K,LIN0,B}	3	184,2	28,1	26,4	25,5	-	-	0,79	0,79	0,76	-	-
M _{K,LIN1,B}	3	167,4	26,9	26,4	26,7	-	-	0,78	0,79	0,75	-	-
M _{K,LIN2,B}	3	210,2	29,9	26,4	23,7	-	-	0,80	0,81	0,75	-	-
M _{0,A}	4	130,4	19,2	19,6	20,2	21,0	-	0,77	0,77	0,77	0,75	-
M _{0,B}	4	130,4	19,2	19,6	20,2	21,0	-	0,77	0,77	0,77	0,75	-
M _{K,LIN0,A}	4	201,4	25,6	22,7	18,9	12,8	-	0,77	0,77	0,77	0,75	-
M _{K,LIN0,B}	4	177,9	23,8	21,6	18,8	15,8	-	0,79	0,80	0,81	0,74	-
M _{K,LIN1,B}	4	158,3	21,9	20,7	19,3	18,1	-	0,78	0,79	0,79	0,75	-
M _{K,LIN2,B}	4	208,7	26,6	22,5	17,8	13,1	-	0,81	0,81	0,82	0,71	-
M _{0,A}	5	125,7	15,9	16,0	16,1	16,1	15,9	0,77	0,77	0,77	0,77	0,75
M _{0,B}	5	125,7	15,9	16,0	16,1	16,1	15,9	0,77	0,77	0,77	0,77	0,73
M _{K,LIN0,A}	5	208,9	23,6	20,8	17,6	13,3	4,7	0,79	0,80	0,80	0,83	1
M _{K,LIN0,B}	5	180,3	22,1	19,5	16,5	12,9	9,0	0,79	0,80	0,80	0,79	0,69
M _{K,LIN1,B}	5	157,6	19,7	18,2	16,4	14,2	11,5	0,78	0,79	0,79	0,79	0,71
M _{K,LIN2,B}	5	216,7	25,9	21,5	16,4	10,4	5,8	0,80	0,82	0,84	0,77	0,63

Table 3 : Results of the shape optimization of the X-Frame with multiple modules

Note that all the optimization and design process only takes a few seconds – or even less – to converge, and convergence could certainly be improved by playing with the parameters of the different algorithms (tolerances, relaxation factors, etc.). For example, with tolerances of 1% on variables for the FSD and OC optimization process, and relaxation factors set to $\eta = 0.5$ and $\tilde{\eta} = 100$, it takes only 2,5 seconds for the model $M_{K,LIN0,B}$ with 5 modules to converge, using a Core i7 2.7-GHz computer with 16 GB memory.

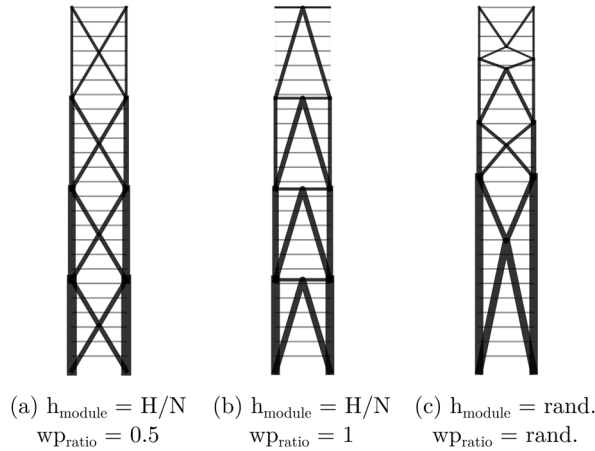


Figure 16 : Initial conditions for the optimization of the multiple modules frame. NB: cross-sectional areas are relative

5. Conclusions

This paper presents the shape optimization of a timber braced frame with dowel-type joints, subject to an overall drift constraint and strength requirements under wind and gravity loads. The main objective of this work is to highlight the impact of joint flexibility on the optimum solution of a truss-like structure. The influence of connections in timber engineering, whether in terms of structural behavior or constructability cannot be overlooked. The development of simplified methodologies that takes into account this specificity remains one of the challenges for structural exploration in the design phase.

The examples presented demonstrate the possible benefits of optimization techniques for the design of braced frame systems for tall buildings. A two-level optimization scheme, using at low-level both FSD (Fully Stressed Design) and a rigorously derived OC (Optimality Criteria) techniques for size optimization, and a more general optimization method for shape optimization has been used. This dissociation allows more control over the optimization process and the use of specialized optimization techniques for each sub-problem.

Our study focuses on a particular unsymmetrical X-braced frame and further work – particularly on other frame geometry – would be needed to generalize the main findings coming from this research presented in section 4, and summarized as follows:

- When the design is controlled by stiffness constraints, the optimal work point of a braced frame module is located near 75% of its height.
- When strength requirements start to control the sizing of columns, the optimal intersection of the diagonals moves down and converges towards 50% for columns with infinite stiffness.
- The introduction of semi-rigid connections has little influence on the optimum work point ratio of the modules, but leads inevitably to a significant increase of the timber volume. This seems to suggest that the number of connections should be reduced to limit the loss of stiffness due to connections in timber structures.
- For a given cross-sectional area, equivalent Young's modulus ratio increases with length. This remark suggests fostering longer members, in line with the previous observation to reduce the number of connections.
- The introduction of semi-rigid connections influences the optimal distribution of modules height, from an equally distributed solution (*i.e.* all the modules have the same height) towards a solution with consecutive modules with decreasing height.

Shape optimization with a continuum geometric domain could lead to solutions with constructability complications. A more restricted design space with construction constraints, for example, allowing the nodes to only be located at floor height, would help rationalize optimal solutions.

As an extension of the work presented here, the topology optimization of braced frameworks for tall buildings, that includes the impact of timber joints, with respect to semi-rigid behavior on structural response, but also on global material costs, could be investigated in future studies.

Acknowledgements

This work was supported by the company Egis Concept (Elioth) and the National Association for Research and Technology (ANRT) within the framework of an industrial agreement for training through research (CIFRE convention number 2017-3577).

Appendix A: Nomenclature

Nomenclature Section 2

Latin upper case letters

A	Cross-section area
E	Timber young's modulus
$F_{v,Rk}$	Characteristic load-carrying capacity per shear plane per fastener
K_c	Connection stiffness for SLS (Service Limit State)
$K_{c,U}$	Connection stiffness for ULS (Ultimate Limit State)
K_{ser}	Slip modulus per shear plane
$K_{ser,p}$	Stiffness of a shear plan
K_w	Apparent stiffness of timber if connection area
L	Length of the member
L_c	Length of the connection
L_{ref}	Length of reference to set the connection compactness
$M_{y,Rk}$	Characteristic yield moment of the connector
$R_{v,Rk}$	Characteristic load-carrying capacity of the connection

Latin lower case letters

d	Dowel diameter
$f_{c,0,k}$	Characteristic compressive strength parallel to grain
$f_{h,1,k}$	Characteristic embedment strength
$f_{t,0,k}$	Characteristic tensile strength parallel to grain
$f_{u,k}$	Ultimate tensile strength of the dowel
k_c	Instability factor
k_{mod}	EC5 strength modification factor
n_1	Number of columns of dowels
n_2	Number of rows of dowels
n_{ef}	Effective number of fasteners in line parallel to the grain
n_{plate}	Number of steel plates
n_{tot}	Total number of dowels
t	Thickness

Greek lower case letters

α	Compactness parameter on connection aspect ratio
β	Compactness parameter on connection length
γ_M	Timber safety factor
η	Cross-section aspect ratio
ρ_m	Mean density of timber

$\sigma_{c,Rd}$	Design compressive stress
$\sigma_{t,Rd}$	Design tensile stress

Nomenclature Section 3

Latin upper case letters	
B	Frame half-width
F_i	Force in member i due to wind load
$F_{W,n}$	External wind force acting at the top of module n
$F_{G,n}$	External dead force acting at the top of module n
$F_{Q,n}$	External live force acting at the top of module n
$F_{Rd,i}$	Design force in element i
H	Frame height
N	Number of modules of the frame
V	Volume of timber in the frame
Latin lower case letters	
f_i^n	force in member i due to a unit load at the top of the n^{th} module
q_w	Wind load pressure
z	Geometry vector of the frame
Greek upper case letters	
Δ_n^j	Displacement at the top of the n^{th} module under a horizontal unit load at the top of the j^{th} module

References

- [1] Foster RM, Ramage MH, Reynolds T. Rethinking CTBUH height criteria in the context of tall timber. CTBUH J 2017;2017:28–33.
- [2] Kuzmanovska I, Gasparri E, Monne DT, Aitchison M. Tall Timber Buildings : Emerging Trends and Typologies. World Conf. Timber Eng. 2018, Seoul, Corea: 2018.
- [3] Ramage MH, Burrige H, Busse-Wicher M, Fereday G, Reynolds T, Shah DU, et al. The wood from the trees: The use of timber in construction. Renew Sustain Energy Rev 2017;68:333–59. doi:10.1016/j.rser.2016.09.107.
- [4] Fleming P, Smith S, Ramage M. Measuring-up in timber: a critical perspective on mid- and high-rise timber building design. Archit Res Q 2014;18:20–30. doi:10.1017/S1359135514000268.
- [5] ADIVbois. Vade-mecum des immeubles à vivre bois. 2017.
- [6] Bendsøe MP, Sigmund O. Topology Optimization. Berlin, Heidelberg: Springer Berlin Heidelberg; 2004. doi:10.1007/978-3-662-05086-6.
- [7] Mijar AR, Swan CC, Arora JS, Kosaka I. Continuum Topology Optimization for Concept Design of Frame Bracing Systems. J Struct Eng 1998;124:541–50. doi:10.1061/(ASCE)0733-9445(1998)124:5(541).
- [8] Liang QQ, Xie YM, Steven GP. Optimal Topology Design of Bracing Systems for Multistorey Steel Frames. J Struct Eng 2000;126:823–9. doi:10.1061/(ASCE)0733-9445(2000)126:7(823).
- [9] Baldock R. Structural Optimisation in Building Design Practice. University of Cambridge, 2007.
- [10] Stromberg LL, Beghini A, Baker WF, Paulino GH. Topology optimization for braced frames: Combining continuum and beam/column elements. Eng Struct 2012;37:106–24. doi:10.1016/j.engstruct.2011.12.034.
- [11] Baker WF. Energy-Based Design of Lateral Systems. Struct Eng Int 1992;2:99–102. doi:10.2749/101686692780615950.
- [12] Beghini LL, Beghini A, Baker WF, Paulino GH. Integrated Discrete/Continuum Topology Optimization Framework for Stiffness or Global Stability of High-Rise Buildings. J Struct Eng 2015;141:04014207. doi:10.1061/(ASCE)ST.1943-541X.0001164.
- [13] Kicinger R, Arciszewski T, DeJong K. Evolutionary Design of Steel Structures in Tall Buildings. J Comput Civ Eng 2005;19:223–38. doi:10.1061/(ASCE)0887-3801(2005)19:3(223).
- [14] Baldock R, Shea K. Structural Topology Optimization of Braced Steel Frameworks Using Genetic Programming. In: Smith IFC, editor. Intell. Comput. Eng. Archit. EG-ICE 2006, LNAI 4200, vol. 4200, Berlin, Heidelberg: Springer Berlin Heidelberg; 2006, p. 54–61. doi:10.1007/11888598.
- [15] Gilbert M, Tyas A. Layout optimization of large-scale pin-jointed frames. Eng Comput 2003;20:1044–64. doi:10.1108/02644400310503017.
- [16] He L, Gilbert M. Rationalization of trusses generated via layout optimization. Struct Multidiscip Optim 2015;52:677–94. doi:10.1007/s00158-015-1260-x.
- [17] Zhang X, Maheshwari S, Ramos AS, Paulino GH. Macroelement and Macropatch Approaches to Structural Topology Optimization Using the Ground Structure Method. J Struct Eng 2016;142:04016090. doi:10.1061/(ASCE)ST.1943-541X.0001524.
- [18] Leichti RJ, Hyde RA, French ML, Camillos SG. The continuum of connection rigidity in timber structures. Wood Fiber Sci

2000;32:11–19.

- [19] Masse DI, Salinas JJ. Analysis of timber trusses using semi-rigid joints. *Can Agric Eng* 1987;111–24.
- [20] Malo KA, Abrahamsen RB, Bjertnæs MA. Some structural design issues of the 14-storey timber framed building “Treet” in Norway. *Eur J Wood Wood Prod* 2016;74:407–24. doi:10.1007/s00107-016-1022-5.
- [21] Lemaître R. Works on Different Numerical modelling Approach to Predict the Load Distribution in Timber Joints. European COST Action FP1402 - Basis of structural timber design - from research to standards. 2018.
- [22] European Committee for Standardization (CEN). Eurocode 5: Design of timber structures - Part 1-1: General - Common rules and rules for buildings 2004.
- [23] Johansen KW. Theory of Timber Connections. *IABSE Int Assoc Bridg Struct Eng* 1949;9:249–62.
- [24] Stepinac M, Cabrero JM, Ranasinghe K, Kleiber M. Proposal for reorganization of the connections chapter of Eurocode 5. *Eng Struct* 2018;170:135–45. doi:10.1016/j.engstruct.2018.05.058.
- [25] Dorn M, de Borst K, Eberhardsteiner J. Experiments on dowel-type timber connections. *Eng Struct* 2013;47:67–80. doi:10.1016/j.engstruct.2012.09.010.
- [26] Reynolds T, Harris R, Chang W. In-service dynamic stiffness of dowel-type connections. 46th Meet. CIB W18 Timber Struct., Vancouver, Canada: 2013. doi:10.13140/2.1.3606.3045.
- [27] Lemaître R, Bocquet J-F, Schweigler M, Bader TK. Beam-on-foundation modelling as an alternative design method for single fastener connections . In: Sandhaas C, Munch-Andersen J, Dietsch P, editors. *Des. Connect. Timber Struct. A state-of-the-art Rep. by COST Action FP1402 / WG3*, Shaker Verlag Aachen; 2018.
- [28] Hochreiner G, Bader TK, Borst K, Eberhardsteiner J. Stiff förmige Verbindungsmittel im EC5 und baustatische Modellbildung mittels kommerzieller Statiksoftware. *Bauingenieur* 2013;88:275–89.
- [29] Sawata K, Yasumura M. Estimation of yield and ultimate strengths of bolted timber joints by nonlinear analysis and yield theory. *J Wood Sci* 2003;49:383–91. doi:10.1007/s10086-002-0497-3.
- [30] Bocquet J-F, Lemaître R, Bader TK. Design recommendations and example calculations for dowel-type connections with multiple shear planes. In: Sandhaas C, Munch-Andersen J, Dietsch P, editors. *Des. Connect. Timber Struct. A state-of-the-art Rep. by COST Action FP1402 / WG3*, 2018, p. 241–95.
- [31] Bocquet J-F, Cabaton L, Calvi D, Sauvignat E. Assemblages bois-métal à plans de cisaillement multiples. Document Technique Plateforme Eurocode 5. 2013.
- [32] Blass HJ, Bejtka I. Self-tapping Screws as Reinforcements in Connections with Dowel-type Fasteners. *Int. Counc. Res. Innov. Build. Constr. CIB-W18 / 38-7-4*, 2005, p. 19.
- [33] Razani R. Behavior of fully stressed design of structures and its relationship to minimum-weight design. *AIAA J* 1965;3:2262–8. doi:10.2514/3.3355.
- [34] Maxwell JC. I.—On Reciprocal Figures, Frames, and Diagrams of Forces. *Trans R Soc Edinburgh* 1870;26:1–40. doi:10.1017/S0080456800026351.
- [35] Michell AGM. LVIII. The limits of economy of material in frame-structures. *London, Edinburgh, Dublin Philos Mag J Sci* 1904;8:589–97. doi:10.1080/14786440409463229.
- [36] Venkayya VB. Design of Optimum Structure. *Comput Struct* 1971;1:265–309. doi:10.1016/0045-7949(71)90013-7.
- [37] Venkayya VB, Berke L, Khot NS. Application of optimality criteria approaches on automated design of large practical structures 1973.
- [38] Fleury C. Structural weight optimization by dual methods of convex programming. *Int J Numer Methods Eng* 1979;14:1761–83. doi:10.1002/nme.1620141203.
- [39] Kirsch U. *Structural Optimization*. vol. 53. Berlin, Heidelberg: Springer Berlin Heidelberg; 1993. doi:10.1007/978-3-642-84845-2.
- [40] Chan C-M, Grierson DE, Sherbourne AN. Automatic Optimal Design of Tall Steel Building Frameworks. *J Struct Eng* 1995;121:838–47. doi:10.1061/(ASCE)0733-9445(1995)121:5(838).
- [41] Chan C-M. Optimal lateral stiffness design of tall buildings of mixed steel and concrete construction. *Struct Des Tall Build* 2001;10:155–77. doi:10.1002/tal.170.
- [42] Powell MJD. A Direct Search Optimization Method That Models the Objective and Constraint Functions by Linear Interpolation. *Adv. Optim. Numer. Anal.*, Dordrecht: Springer Netherlands; 1994, p. 51–67. doi:10.1007/978-94-015-8330-5_4.
- [43] Jones E, Oliphant T, Peterson P. *SciPy: Open Source Scientific Tools for Python* 2001.